

Design and Analysis of an Artificial Finger Joint for Anthropomorphic Robotic Hands

Zhe Xu, Emanuel Todorov, Brian Dellon and Yoky Matsuoka

Abstract—In order to further understand what physiological characteristics make a human hand irreplaceable for many dexterous tasks, it is necessary to develop artificial joints that are anatomically correct while sharing similar dynamic features. In this paper, we address the problem of designing a two degree of freedom metacarpophalangeal (MCP) joint of an index finger. The artificial MCP joint is composed of a ball joint, crocheted ligaments, and a silicon rubber sleeve which as a whole provides the functions required of a human finger joint. We quantitatively validate the efficacy of the artificial joint by comparing its dynamic characteristics with that of two human subjects' index fingers by analyzing their impulse response with linear regression. Design parameters of the artificial joint are varied to highlight their effect on the joint's dynamics. A modified, second-order model is fit which accounts for non-linear stiffness and damping, and a higher order model is considered. Good fits are observed both in the human ($R^2 = 0.97$) and the artificial joint of the index finger ($R^2 = 0.95$). Parameter estimates of stiffness and damping for the artificial joint are found to be similar to those in the literature, indicating our new joint is a good approximation for an index finger's MCP joint.

I. INTRODUCTION

Due to its inherent similarity with the human hand anthropomorphic robotic hands have the potential to beneficially impact many aspects of people's lives. Areas such as space exploration, personal assistance, and hand prosthetics can all be better served with a highly biomimetic artificial hand. Space exploration relies on constant repair of orbiting, or space-bound, platforms where exploration in and of itself is often dangerous for humans requiring highly dexterous robotic manipulators to function in their place. Achieving a robotic hand with characteristics closely resembling our own will allow natural interaction while enabling a leap in prosthetic design. But significant challenges must first be overcome. These challenges include matching the same degrees of freedom (DOFs) of the human hand, possibly for restoring hand dexterity and functions, and also replicating human finger compliance to allow safe operation in unstructured human environments. Other large technical obstacles also exist in terms of power, actuation, and weight constraints. However, here we focus on the intrinsic biomechanics required to replicate a human finger joint.

The finger joints in the human hand possess several biological features that are hard to mimic simultaneously. These include: (1) the unique shape of the bones at the MCP, PIP

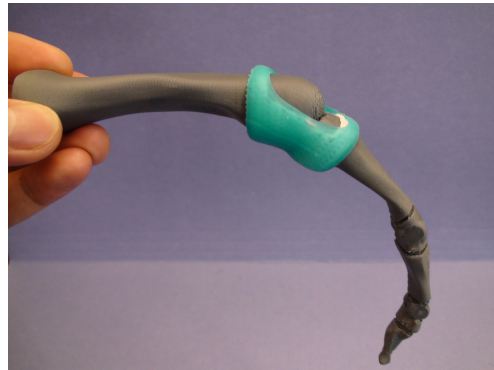


Fig. 1. Compliant artificial finger joint with true to life bone shapes

and DIP joints, which determines the degrees of freedom at the joint; (2) a joint capsule formed by fine ligaments, which set the range of motion for the joint; and (3) cartilage and synovial fluid, enabling low-friction contact between two articulated surfaces [1]. Typically researchers have not designed anthropomorphic robotic hands to incorporate these biological features or to be anatomically correct.

There are two types of joint designs that have been widely used in anthropomorphic robotic hand research. The first type uses standard mechanical components such as hinges, gimbals, linkages, or gears and belts [2]–[12]. Several important features have been achieved in these anthropomorphic robotic hands, including high degrees of modularity [7], built-in actuators [5], [7]–[9], low inertia [5], [8], [13], and extra palmar DOFs [4], [6]. While this methodology promises excellent performance in achieving the right number of DOFs and even mimicking kinematic characteristics of the human finger, it involves considerable systems-level complexity and implementation costs. In addition few of these types of hands possess built-in compliance which is necessary for a human hand to explore uncertainties in the unstructured real world.

An alternative approach to joint coupling uses a simplified design with passive compliance for adaptability. These types of hands are often under-actuated [13]–[16], with fewer actuators than degrees of freedom, and therefore reduce overall complexity of the robotic hand's mechanisms. Mechanical compliance is perhaps the simplest way to allow for coupling between joints without enforcing the fixed-motion coupling relationship inherent with gears or linkages. The hand/graspers made in this way often have superior robustness properties and are able to withstand large impacts without damage [16]. But

Authors are with the Department of Computer Science & Engineering, University of Washington, WA 98195, USA
e-mail: zhexu@cs.washington.edu, todorov@cs.washington.edu, Btd@cs.washington.edu, yoky@cs.washington.edu

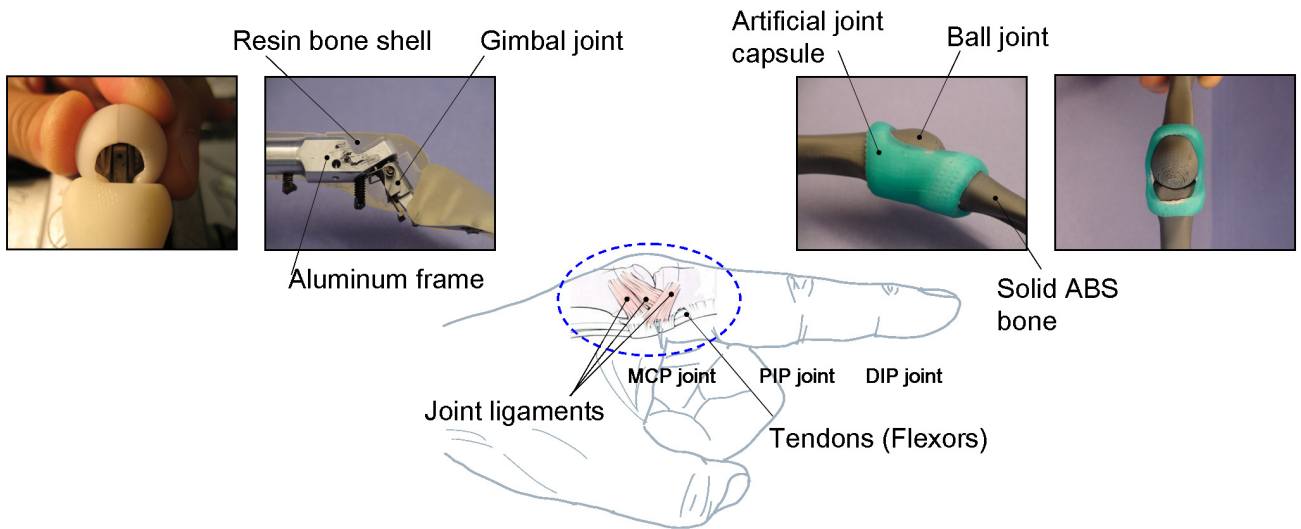


Fig. 2. Comparison of the MCP joint design between the current and new version of the ACT Hand

there is also a tradeoff between achieving the desired range of motion of the finger and having a compliant finger joint since the elastic component cannot by itself limit the joint's range of motion.

Although standard design methodology, such as above, can mimic the kinematic behavior of a finger joint it does little to illuminate the salient features that make the human hand irreplaceable for many dexterous tasks. It is therefore necessary to develop artificial finger joints, based on accurate physiology, in order to quantitatively identify these characteristics thus providing insight into anthropomorphic robotic hand design.

A compelling alternative to standard mechanical components is to develop mechanisms which directly utilize the unique articulated shapes of human joints, as well as a tendon hood structure to actuate the finger. Following a biologically inspired design also reduces the total number of individual components, resulting in an elegant design.

The finger joint described in this paper is inspired by the combination of the above approaches and has the potential to become an essential component for the next generation of the Anatomically Correct Testbed (ACT) hand [17]–[19]. We focus on the joint capsule and present an artificial joint whose mechanical design and range of motion is similar to that of the human finger. In the following sections the innovative mechanical design methods are detailed, then the system dynamics of our artificial MCP joint are compared with an actual human finger's MCP joint.

II. DEVELOPMENT OF AN ARTIFICIAL FINGER JOINT

The artificial joint discussed in this paper is inspired by the current version of the ACT Hand. Due to a common ancestor from a cadaver hand both joints share many biomechanical features such as the length of the bone sections, shape of the joint surfaces, and extensor hood. However, there are key differences between the two.

In Figure 2, the metacarpophalangeal (MCP) joint of the ACT Hand's index finger for both the current and new design are compared with the human counterpart. The anatomical drawing of Figure 2 shows the MCP joint with the extensor hood removed. The current version of the ACT Hand uses a gimbal joint to realize 2-DOF at the MCP joint ($\pm 35^\circ$ for adduction/abduction, -30° to 90° for extension/flexion). While the artificial joint uses a solid sphere which is close to that of a human finger to realize the 2-DOF finger motion (with one extra under-actuated DOF from the 3DOF spherical joint). Our artificial joint is designed independently from the extensor hood, thus does not fully cover the upper portion of the MCP joint, this can be seen in the right hand side of Figure 2.

As shown in the leftmost picture of Figure 2, the range of motion of the index finger in the current design of the ACT Hand is prescribed by the shape of the MCP bone shell. While the new design uses crocheted joint ligaments to limit the range of motion of the MCP joint with an elastic sleeve to replicate passive biomechanics of the musculo-skeletal structure. Although the kinematics of the MCP joint in the current version of the ACT hand matches the human hand very well, a complex motor control strategy must be used in order to simulate the passive biomechanics. Shifting the load of simulating passive biomechanics into physical elastic elements at the joints will allow the ACT hand to reduce its control complexity. This not only saves power but also lowers the chance of saturating the actuators with non task-specific commands.

In the following subsections, each of the components of the artificial joint will be introduced according to its assembly sequence.

A. Modular design of the finger

The adoption of an anatomically correct bone structure would seem to imply a cost intensive and complex manufac-

turing process. However this cost can be side stepped through the innovation of rapid prototyping machines. Each section of the finger joint is 3D printed by the Dimension BST 768 (Stratasys Corp., Eden Prairie, MN). The resolution of the 3D printed parts is 0.025mm, and it takes only 3 hours to print all the components of the entire index finger. Additionally the strength of the ABS plastic is sufficient to resist the induced stress of the extensor hood.

Each distal section of the finger joint is designed to be detachable from its base as shown in Figure 3 (a). This design serves two functions. The first is for easily mounting a steel ring (0.8mm in diameter) whose shape conforms to the contour of the cross section of the ABS bone. The rim of the crocheted joint capsule is sewn onto this steel ring (Figure 3 (b)) so that the latter forms a continuous attachment zone for the former part along the contour of the cross section near the finger joint. A partially assembled MCP joint section is shown in Figure 3 (c).

The second function of this modular design is to provide a platform for future improvement. For instance, the surface of the ABS parts can be further plated with a 0.003 inch thickness of chrome to provide a better approach to frictionless contact at the finger joint (RePliForm Corp., Baltimore, MD). An instant benefit of this design is also demonstrated in the experimental section where different weights of the distal finger are tested for dynamic identification.

In order to mimic the frictionless surface of the articulated cartilage of the human joint a thermoplastic (Shapelock Corp., Sunnyvale, CA) was used to coat the surface of the socket side of the MCP joint as shown in Figure 3 (d). This combination of the joint coupling decreases the friction between the two articulated surfaces.

B. Crocheted joint ligaments

The joint capsule is a dense fibrous connective tissue that is attached to the bones via specialized attachment zones and forms a sleeve around the joint. It varies in thickness according to the stresses to which it is subject, and is locally thickened to form capsular ligaments, which may also incorporate tendons (Figure 2). It seals the joint space and provides passive stability by limiting movements through its ligaments [20].

In hand surgery surgeons avoid using mechanically complicated replacements for finger joints. Common prosthetic joints used in hand surgery may include flexible segments made either from titanium alloys, ceramics, or plastics [21] but do not replicate the surface details found on the bone ends. The flexible segments of the prosthetic joint are inserted into holes created inside of neighboring phalanges. The joint is then sealed with the joint capsule. These types of artificial joints have been clinically proven to restore joint function [22]. Without the joint capsule the neighboring phalanges would lose integrity and fall apart, thus it is a critical component of our biologically inspired artificial joint.

Our crocheted joint ligaments are fabricated with 0.46mm Spectra® fiber (AlliedSignal, Morristown, NJ). The fiber was chosen because of its strength (200N breaking strength), high

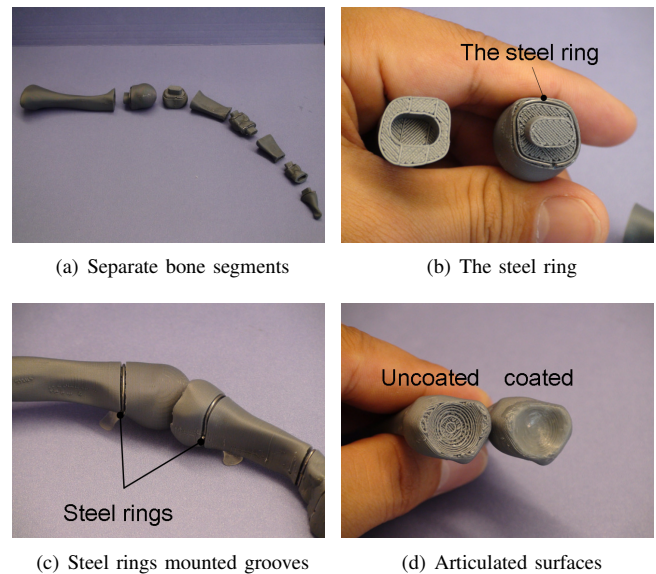


Fig. 3. Components of the index finger bones. (a) Modular design of the index finger. (b) & (c) Steel rings used to anchor the rim of the crocheted finger capsule. (d) Thermoplastic coated articulated surface providing low-friction surface at the finger joint.

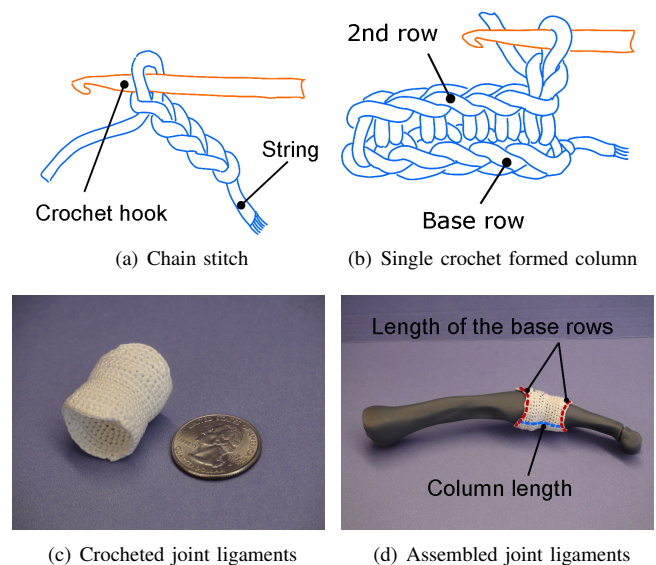


Fig. 4. Crocheted ligaments of the MCP joint. (a) Basic crochet type I – chain stitch. (b) Basic crochet type II – single crochet. (c) Hyperbolic shape of crocheted joint ligaments limits the range of motion of the MCP joint of the index finger. (d) Partially assembled index finger with crocheted ligaments attached.

stiffness, flexibility, and its ability to slide smoothly over the bones.

Two basic crochet stitches were applied during the fabrication of the artificial ligaments. These are the *chain stitch* and *single crochet* as shown in Figure 4 (a) and (b). A series of chain stitches is called a *row*, the length of the row is determined by the local perimeter of the joint capsule. A single crochet determines the row width, while a double crochet would increase this width. The total width of the chains formed

by single crochet becomes the *column length* of the joint capsule.

A sample of crocheted joint ligaments is shown in Fig 4 (c) and (d). This sample illustrates the full hyperbolic shape [23], which covers the area where the extensor hood is typically located. Our design (shown in Figure 2) excludes this dorsal area because we consider the extensor hood to be an independent component [24]. The hyperbolic shape of the crocheted ligament is well suited for sealing the joint space, and its column length determines the range of motion of the MCP joint.

Given a fixed distance between the two steel rings the column length then determines the amount of slack in the ligaments with the joint in a neutral position. This slack from the crocheted ligaments constrains the joint's range of motion as it moves. The column length was empirically determined based on the dimension of the joint. The base row for each end of the joint ligaments is formed by a chain whose total length is equal to the perimeter of the steel ring. The local thickness of the joint capsule can also be controlled by varying the stitch type. After fabricating the crocheted joint capsule, it is sewn onto the steel ring which snaps into a groove cut into the bone.

C. Silicon rubber sleeve

Dynamic properties of the finger joints are largely determined by the passive biomechanics of the muscles and tendons which route along the bone surfaces. Rather than mimic the musculo-skeletal properties with an actuator an elastic sleeve can be designed to act on each joint in combination with the crocheted ligaments, recreating the intended dynamics.

The elastic component of the artificial joint is made of silicon rubber (PlatSil[®] 71 Series RTV, Polytek Development Corp., Easton, PA) with high shear strength. Its shape is cast by a set of 3D printed molds (see Figure 5) which forms a sleeve around the MCP joint providing elastic and viscous forces during finger flexion/extension.

To achieve optimal performance of the silicon rubber, a vacuum chamber was used to remove tiny air bubbles from the silicon mixture before curing. The thickness of the silicon rubber sleeve can be easily modified by using different molds. This feature provides adjustable stiffness and damping for the artificial joint capsule for our dynamic identification.

Together, all of the above components set the stage to enable the artificial finger joint to closely mimic the kinematics and dynamics of the human joint. In order to validate the efficacy of our approach, we conducted system identification of the artificial joint.

III. SYSTEM IDENTIFICATION

We performed a set of experiments and analyses aimed at identifying the dynamic properties of our new robotic joint, as well as comparing it to a human finger.

The experimental setup is illustrated in Fig 6. We performed experiments with two human subjects as well as four different artificial fingers. The latter differed by the thickness of the silicon material (thin 1.5 mm vs. thick 2.0 mm), and the

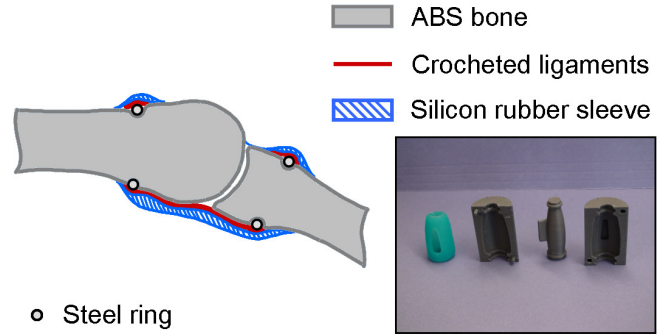


Fig. 5. Cross section of the fully assembled MCP joint. *Bottom Right:* The silicon rubber sleeve and the molds used for its fabrication.

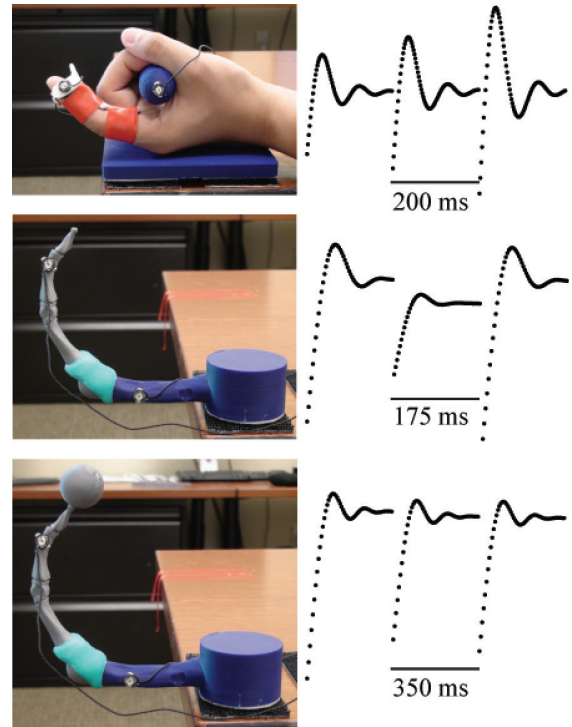


Fig. 6. Left: Experimental setup. Right: typical trials for each finger, using the thick silicon cover.

presence or absence of a 7.5g mass added to the distal segment (8.7g). All four combinations were studied. Infrared markers (PhaseSpace Inc., San Leandro, CA) were attached to the base and distal segments of each finger. The 3D marker coordinates were measured at 480 Hz using a 7-camera system. The base of the hand was immobilized as shown in the figure. The DIP and PIP joints of the human finger were also immobilized; the artificial finger did not have movable DIP and PIP joints. The human subjects were instructed to relax and close their eyes, so as to avoid voluntary responses as much as possible.

A. Experimental design and methods

The protocol included about 120 perturbations applied manually, at roughly 1s intervals. In each perturbation the

experimenter extended the finger (human or artificial) to a randomly chosen position, and suddenly released it. The motion capture data was recorded continuously and parsed into individual trials offline. This design aimed to reveal the dynamic properties of the fingers around the point of stopping. The rationale was that, if the fingers behaved like mass-spring-damper systems [25], the stopping phase would be particularly revealing with regard to their dynamic properties.

B. Data processing

The raw data was very clean. The noise standard deviation in static conditions was on the order of 50 microns (0.05 mm) without filtering. Since we needed up to 3rd derivatives of position, we fit a cubic spline (Matlab Spline toolbox) and adjusted its smoothing parameter so that it did not introduce artefacts in the raw position data and yet the high-order derivatives were smooth. We then implemented a procedure that automatically identified the individual trials in the continuous record, using the fact that once the finger was released, it developed a high velocity due to the passive stiffness. Trial onset was thus defined as the peak of the flexion velocity – so as to avoid contamination due to forces applied by the experimenter. We included in the dataset a certain time interval after each velocity peak: 175 msec for the unloaded artificial fingers, 350 msec for the loaded artificial fingers, and 200 msec for the human fingers. These were adjusted so as to capture the different timescales apparent in the data. 100 trials per condition were included in the dataset. Since the results for the two human subjects were very similar but we collected less usable data for one of them, we focus on the data for the other subject. Typical trials are illustrated in Fig 6.

The 3D position of the distal marker was converted to radians as follows. Using Principal Components Analysis we identified the 2D plane in which the marker was moving; there was actually some movement in the third dimension as well, but we verified visually that the main movement was in the 2D plane defined in our analysis. We then fit a circle to the projected 2D data, using the known distance between the MCP joint center and the distal marker. This distance was measured with a caliper in the human subjects, and was known from the CAD model in the artificial finger.

C. Qualitative observations

Subjectively, the artificial finger felt a lot like a relaxed human finger. The trials in Fig 6 illustrate that all systems had slightly under-damped behavior (more so for the human finger). Another similarity was that both the artificial and human fingers had nonlinear stiffness which rapidly increased near the joint limit. We plan to quantify this effect in future work using a force probe.

There were also differences. The unloaded artificial finger came to an abrupt stop, which a mass-spring-damper cannot do. Instead this behavior suggests a certain amount of friction – which can also explain why the artificial finger reached different equilibrium positions on different trials.

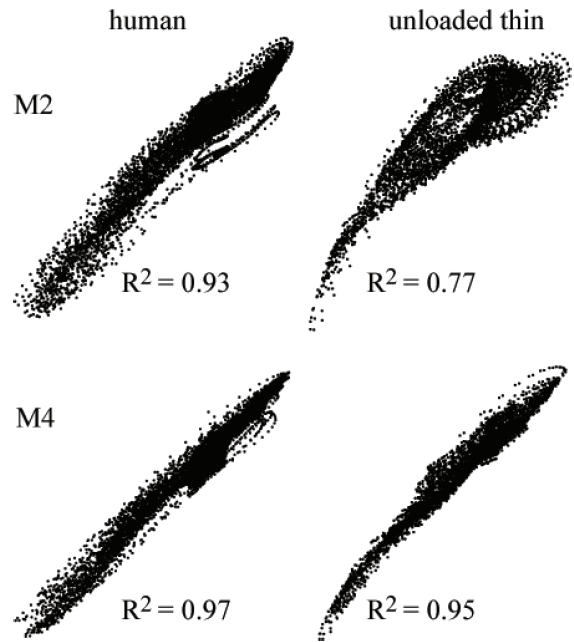


Fig. 7. Measured vs. predicted acceleration for models M2 and M4, human and artificial fingers (unloaded thin).

D. Quantitative results

1) *Second-order models:* All models were fit using linear regression (Matlab Statistics toolbox), and all fits reported in the paper and summarized in Table I were significant ($p < 0.05$).

We first fit a simple mass-spring-damper model (model M1) to all datasets:

$$\ddot{\theta} = -k\theta - b\dot{\theta} + a_0 + a_1 \cos(\theta) + a_2 \sin(\theta) \quad (M1)$$

This model was chosen because we did not have inertial measurements for the human finger (and were not entirely confident in the CAD estimates for the artificial finger either). Thus k, b here are the stiffness and damping coefficients divided by the moment of inertia. The term a_0 accounts for the spring reference point, as well as any other potential biases. The trigonometric terms account for gravitational forces.

TABLE I
R² COEFFICIENTS FOR ALL MODELS AND DATASETS

	M1	M2	M3	M4
Human	0.92	0.93	0.89	0.97
Unloaded thick	0.63	0.74	0.90	0.94
Unloaded thin	0.69	0.77	0.91	0.95
Loaded thick	0.50	0.55	0.91	0.71
Loaded thin	0.39	0.40	0.87	0.60

Model M1 fit the human data quite well, but provided a rather poor fit (Table I) for all artificial fingers, indicating that the latter dynamics are more complex. In an attempt to improve the fit we then constructed the extended model M2:

$$\ddot{\theta} = -k\theta - b\dot{\theta} + a_0 + a_1 \cos(\theta) + a_2 \sin(\theta) + c_1 \tanh(\dot{\theta}) + c_2\dot{\theta}^2 + c_3\dot{\theta}^2 \quad (\text{M2})$$

The quadratic terms $\theta^2, \dot{\theta}^2$ were added so as to allow nonlinear stiffness and damping. The sigmoid (tanh) term was included as a model of friction. This extension improved the fits somewhat but the results for the artificial fingers were still disappointing. The measured vs. predicted accelerations from model M2 are shown in Fig 7 top. Note that the artificial finger data has an interesting residual structure. We experimented with other nonlinear terms of position and velocity but could not improve the results significantly.

2) *Third-order models*: The above difficulties indicated that the acceleration of the artificial finger may not be a well-defined function of position and velocity, but instead the system may have higher-order dynamics. Plotting the raw data as a 3D scatter plot confirmed our suspicion. Two projection of this 3D plot are shown on the top of Fig 8. It is clear that the surface often has two different accelerations for the same point in position-velocity space.

We therefore re-analyzed the data under the assumption of 3rd-order dynamics. Fig 8 bottom shows the 3D scatter plot of jerk (derivative of acceleration) as a function of velocity and acceleration. We now observe that this function is well-defined (even though there are some positional effects not included in the figure). This prompted us to fit the following regression model, predicting the instantaneous jerk rather than acceleration:

$$\ddot{\theta} = w_0 + w_1\theta + w_2\dot{\theta} + w_3\ddot{\theta} + w_4 \tanh(\dot{\theta}) \quad (\text{M3})$$

The sigmoid term is motivated by the fact that the surface has different behavior near zero velocity. As can be seen in Table I, model M3 fit all datasets rather well. We then went back to the acceleration-based model (M2) and asked how it can be improved. Integrating M3, it is clear that model M2 can be improved by adding a state variable which is the integral of the sigmoid term, namely

$$\psi(t) = \int_0^t \tanh(\dot{\theta}(\tau)) d\tau$$

Thus our final acceleration-based model is

$$\ddot{\theta} = -k\theta - b\dot{\theta} + a_0 + a_1 \cos(\theta) + a_2 \sin(\theta) + c_1\psi + c_2\dot{\theta}^2 + c_3\dot{\theta}^2 \quad (\text{M4})$$

This model provided a very good fit for the unloaded artificial fingers (see Table I and Fig 7). Thus the artificial finger has higher-order dynamics, presumably due to systematic movement of the joint capsule material relative to the segments. Interestingly, model M4 did not work so well for the loaded finger – indicating that the added mass interacts with this higher-order dynamics in some nontrivial way. Understanding this effect in more detail will be left for future work. To obtain

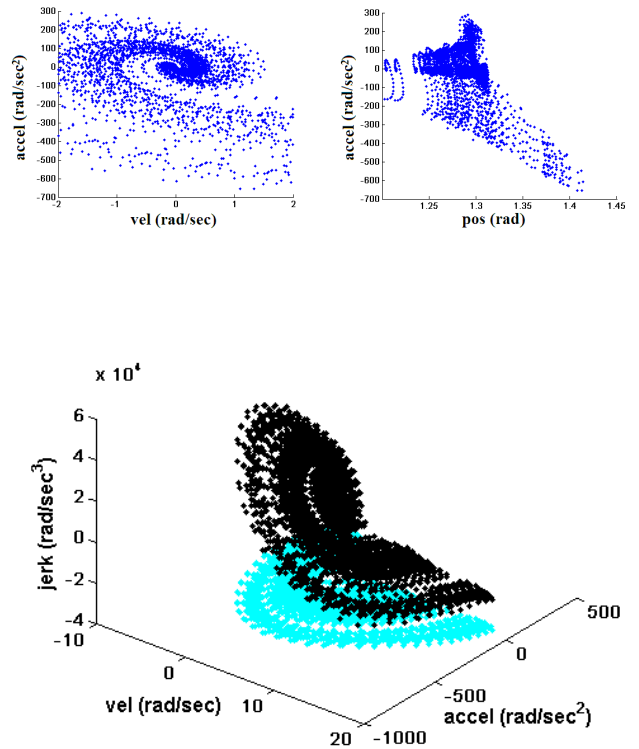


Fig. 8. Top: scatter plots of acceleration vs. position and velocity. Bottom: 3D scatter plot of jerk vs. velocity and acceleration. The light dots are the projection of the data on the bottom plane. All data in this figure is from the artificial finger (unloaded thin).

values for stiffness and damping that can be compared to the values estimated for human finger in [25], a simplified version of model M4 is constructed by removing the quadratic and trigonometric terms. We used an inertia of $0.0006 \text{ kg} \cdot \text{m}^2$ for the unloaded finger (Estimated in Pro/E model) and averaged the results for the thick and thin capsules and the unloaded condition. The comparison is shown in Table II, the values are quite similar indicating our artificial joint has similar stiffness and damping.

TABLE II
COMPARISON OF STIFFNESS & DAMPING FOR THE HUMAN AND ARTIFICIAL MCP JOINTS

MCP joint of the index finger	Stiffness K (Nm/rad)	Damping B (Nms/rad)
Human joint	0.50 (averaged between -0.2 to 1 radians)	0.0142 (SD = 0.23)
Artificial joint	0.534 +/- 0.025 (95% confidence interval)	0.024 +/- 0.0003 ($R^2 = 0.87$)

IV. CONCLUSION

We have described the design and modeling of an artificial finger joint that has the potential to become a close replica

of the MCP joint in the human hand. The artificial joint makes use of three main components: a ball joint with true to life bone topology, crocheted ligaments used to realize the right range of motion, and a silicon rubber sleeve providing the passive compliance for the artificial joint. For our system identification, two key design parameters were investigated to optimize the models derived for the MCP joint of the index finger. The model is in good agreement with the data collected from both the MCP joint of the artificial and human index fingers. We expect to apply a similar design to both the PIP and DIP joints and have already designed and fabricated an extensor tendon hood so that the whole artificial finger will eventually be controlled by a series of extensors and flexors in the same way as a human hand. We also believe that a deeper understanding of the unique features in human hands will provide greater insight into future designs of anthropomorphic robotic hands.

REFERENCES

- [1] P. W. Brand and M. H. Anne, *Clinical Mechanics of the Hand*. St. Louis: Mosby-Year Book, Inc., 1993.
- [2] G. Bekey, R. R. Tomovic, and I. Zeljkovic, "Control architecture for the belgrade/USC hand," *Dextrous Robot Hands*, pp. 136–149, 1990.
- [3] S. Jacobsen, E. Iversen, D. Knutti, R. Johnson, and K. Biggers, "Design of the Utah/M.I.T. dextrous hand," vol. 3, pp. 1520–1532, Apr 1986.
- [4] C. Lovchik and M. Diftler, "The Robonaut hand: a dexterous robot hand for space," in *Proceedings of the 1999 IEEE International Conference on Robotics and Automation*, vol. 2, 1999, pp. 907–912.
- [5] T. Mouri, H. Kawasaki, Y. Keisuke, J. Takai, and S. Ito, "Anthropomorphic robot hand: Gifu hand III," *Proc. Int. Conf. ICCAS*, p. 1288, 2002.
- [6] Shadow Robot Company, "www.shadowrobot.com," 2008.
- [7] Butterfass, J. and Fischer, M. and Grebenstein, M. and Haidacher, S. and Hirzinger, G., "Design and experiences with DLR hand II," vol. 15, 2004, pp. 105–110.
- [8] I. Yamano and T. Maeno, "Five-fingered robot hand using ultrasonic motors and elastic elements," in *Proceedings of the 2005 IEEE International Conference on Robotics and Automation*, April 2005, pp. 2673–2678.
- [9] J. Ueda, Y. Ishida, M. Kondo, and T. Ogasawara, "Development of the NAIST-Hand with vision-based tactile fingertip sensor," April 2005, pp. 2332–2337.
- [10] M. C. Carrozza, G. Cappiello, S. Micera, B. B. Edin, L. Beccai, and C. Cipriani, "Design of a cybernetic hand for perception and action," *Biol. Cybern.*, vol. 95, no. 6, pp. 629–644, 2006.
- [11] Touch Bionics Inc., "www.touchbionics.com," 2009.
- [12] DEKA Research and Development Corp., "www.dekaresearch.com," 2008.
- [13] F. Lotti, P. Tiezzi, G. Vassura, L. Biagiotti, G. Palli, and C. Melchiorri, "Development of UB Hand 3: Early results," in *Proceedings of the 2005 IEEE International Conference on Robotics and Automation*, April 2005, pp. 4488–4493.
- [14] P. J. Kyberd, C. Light, P. H. Chappell, J. M. Nightingale, D. Whatley, and M. Evans, "The design of anthropomorphic prosthetic hands: A study of the southampton hand," *Robotica*, vol. 19, no. 6, pp. 593–600, 2001.
- [15] M. C. Carrozza, C. Suppo, F. Sebastiani, B. Massa, F. Vecchi, R. Lazzarini, M. R. Cutkosky, and P. Dario, "The spring hand: Development of a self-adaptive prosthesis for restoring natural grasping," *Autonomous Robots*, vol. 16, no. 2, pp. 125–141, 2004.
- [16] A. Dollar and R. Howe, "Simple, robust autonomous grasping in unstructured environments," in *2007 IEEE International Conference on Robotics and Automation*, April 2007, pp. 4693–4700.
- [17] D. Wilkinson, M. Vande Weghe, and Y. Matsuoka, "An extensor mechanism for an anatomical robotic hand," vol. 1, Sept. 2003, pp. 238–243 vol.1.
- [18] M. Vande Weghe, M. Rogers, M. Weissert, and Y. Matsuoka, "The ACT hand: Design of the skeletal structure," in *Proceedings of the 2004 IEEE International Conference on Robotics and Automation*, 2004.
- [19] L. Y. Chang and Y. Matsuoka, "A kinematic thumb model for the ACT hand," in *Proceedings of the 2006 IEEE International Conference on Robotics and Automation*, 2006.
- [20] J. R. Ralphs and M. Benjamin, "The joint capsule: structure, composition, ageing and disease," *Journal of Anatomy*, vol. 3, pp. 503–509, 1994.
- [21] T. Joyce, "Currently available metacarpophalangeal prostheses: their designs and prospective considerations," *EXPERT REVIEW OF MEDICAL DEVICES*, vol. 1, no. 2, pp. 193–204, NOV 2004.
- [22] D. Beevers and B. Seedhom, "Metacarpophalangeal joint prostheses: A review of the clinical results of past and current designs," *The Journal of Hand Surgery: Journal of the British Society for Surgery of the Hand*, vol. 20, no. 2, pp. 125 – 136, 1995.
- [23] D. Henderson and D. Taimina, "Crocheting the hyperbolic plane," *MATHEMATICAL INTELLIGENCER*, vol. 23, no. 2, pp. 17–28, SPR 2001.
- [24] F. H. Netter, *Atlas of Human Anatomy*, 2nd ed. Teterboro, New Jersey: Icon Learning Systems, 1997.
- [25] D. G. Kamper, T. G. Hornby, and W. Z. Rymer, "Extrinsic flexor muscles generate concurrent flexion of all three finger joints," *Journal of Biomechanics*, vol. 35, no. 12, pp. 1581 – 1589, 2002.